Proton Radiation Effects on Electronic Defect States in MOCVD-Grown (010) β-Ga2O3

McGlone, Ghadi, Cornuelle, Armstrong, Burns, Feng, Bhuiyan, Zhao, Arehart, and Ringel

Proton Radiation Effects on Electronic Defect States in MOCVD-Grown (010) β-Ga_2O_3

Joe F. McGlone,[1, a)] Hemant Ghadi,[1, a)] Evan Cornuelle,[1] Andrew Armstrong,[2] George Burns,[2] Zixuan Feng,[1] A F M Anhar Uddin Bhuiyan,[1] Hongping Zhao,[1,3] Aaron R. Arehart,[1] and Steven A. Ringel[1,3, b)]

[1)] *Department of Electrical and Computer Engineering, The Ohio State University, Columbus, OH 43210, USA*

[2)] *Sandia National Laboratories, Albuquerque, NM 87123, USA*

[3)] *Department of Materials Science and Engineering, The Ohio State University, Columbus, OH 43210, USA*

(Dated: January 4, 2023)

The impact of 1.8 MeV proton irradiation on metalorganic chemical vapor deposition (MOCVD) grown (010) β-Ga_2O_3 Schottky diodes is presented. It is found that after a 10.8×10^{13} cm^{-2} proton fluence the Schottky barrier height of (1.40 ± 0.05 eV) and the ideality factor of (1.05 ± 0.05) are unaffected. Capacitance-voltage extracted net ionized doping curves indicate a carrier removal rate of 268 ± 10 cm^{-1}. The defect states responsible for the observed carrier removal are studied through a combination of deep level transient and optical spectroscopies (DLTS/DLOS) as well as lighted capacitance-voltage (LCV) measurements. The dominating effect on the defect spectrum is due to the E_C-2.0 eV defect state observed in DLOS and LCV. This state accounts for $\sim$75% of the total trap introduction rate and is the primary source of carrier removal from proton irradiation. Of the DLTS detected states, the E_C-0.72 eV state dominated but had a comparably smaller contribution to the trap introduction. These two traps have been previously correlated with acceptor-like gallium vacancy-related defects. Several other trap states at E_C-0.36 eV, E_C-0.63 eV, E_C-1.09 eV were newly detected after proton irradiation, and two pre-existing states at E_C-1.2 eV and E_C-4.4 eV showed a slight increase in concentration after irradiation, together accounting for the remainder of trap introduction. However, a pre-existing trap at E_C-0.40 eV was found to be insensitive to proton irradiation and therefore is likely of extrinsic origin. The comprehensive defect characterization of 1.8 MeV proton irradiation damage can aid the modeling and design for a range of radiation tolerant devices.

I. Introduction

Gallium oxide in its beta phase (β-Ga_2O_3) has compelling material properties that have generated a large and growing interest for applications in high-voltage and high-power RF electronics and ultraviolet optoelectronics. Availability of low-cost, large-area, melt-grown bulk substrates[1–4] has fueled interested in the β-Ga_2O_3 material system. However, the main driver for the growing interest is the ultra-wide bandgap (UWBG) reported to be $\sim$4.6-4.8 eV.[5–7] The UWBG leads to a large breakdown field that increases the Baliga and Johnson figures of merit, indicating potentially superior performance in high-power and high-frequency devices compared to more contemporary wide bandgap semiconductors such as GaN or SiC.[8–10] The UWBG also offers advantages for device applications in environments with high energy particle radiation, such as space communication applications or radiation hard devices and detectors in nuclear energy. Larger bandgap materials are generally associated with smaller lattice constants with higher bond strengths, giving them a propensity for better radiation hardness. This is predicted from an empirical relationship between the inverse of the lattice constant and the displacement energy.[11]

Radiation effects on β-Ga_2O_3 with different growth techniques such as halide vapor phase epitaxy (HVPE), molecular beam epitaxy (MBE), and edge-defined film fed growth (EFG) using proton, neutron, electron, and alpha radiation have been studied.[12–21] However, radiation effects on metalorganic chemical vapor deposition (MOCVD) grown β-Ga_2O_3 are unexplored. The current status of the commercially viable MOCVD growth technique has already proven to be capable of generating high-mobility material with a low background of compensating acceptor defects[22–25], which has accelerated the promise of significant impact for β-Ga_2O_3 and the MOCVD growth technique for high quality devices. Previous work by Ghadi *et al.* demonstrated the remarkably low defect concentrations in β-Ga_2O_3 grown via MOCVD.[24,25] The high quality material with low defect concentrations allows for a high sensitivity to newly formed defects or increases in the concentrations of defects that exist before radiation, making it ideal to study radiation effects. Additionally, radiation damage tends to create defects having an intrinsic character (including complexes with elements such as H), whereas existing extrinsic defects are not expected to be significantly influenced by radiation effects, thereby aiding in differentiating between intrinsic and extrinsic defect sources.

This work presents a comprehensive and quantitative study of defect states created by 1.8 MeV proton irradiation of β-Ga_2O_3 epitaxial layers grown by MOCVD on β-Ga_2O_3 substrates. Both deep level transient spectroscopy (DLTS) and deep level optical spectroscopy (DLOS) measurements are used to reveal the distribution of individual trap concentrations throughout the entire bandgap as a function of proton irradiation fluence. Comparative analyses on the individual defect introduction rates are made to observe defect

[a)] J. F. McGlone and H. Ghadi contributed equally to this work.

[b)] Authors to whom correspondence should be addressed: mcglone.55@osu.edu, ringel.5@osu.edu

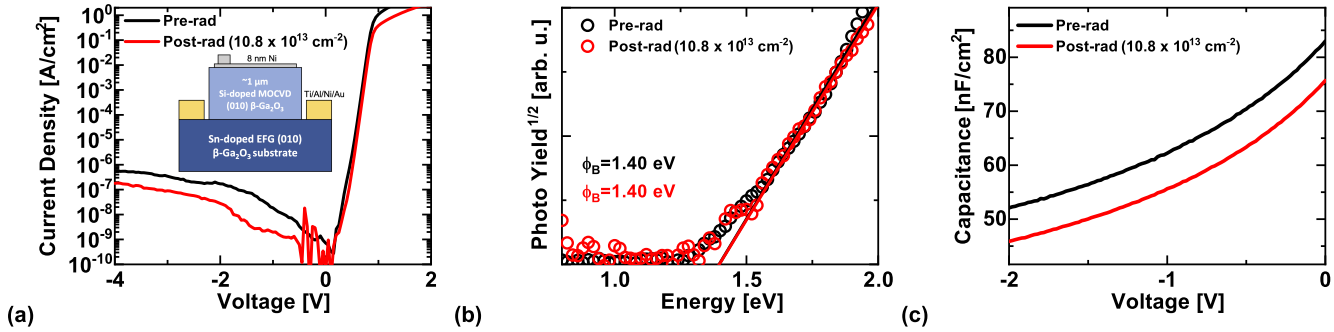

Figure 1. (a) shows the I-V characteristics of the same device at each proton radiation condition. The device cross-sectional diagram is shown in the inset. A reduction in leakage current and a decrease in on current is observed due to the radiation damage. (b) shows the internal photo-emission characterization with a negligible change in the measured Schottky barrier height. (c) shows the C-V curves for the same device with a reduction in capacitance due to radiation damage.

formation, and the relative impact of each defect state on critical electrical properties that can influence devices, such as carrier compensation.

II. Growth and Processing

The epitaxial layer used as the basis for this study was grown on a conductive Sn doped (010) EFG (edge-defined film fed growth) substrate from Novel Crystal Technology. An Agnitron Agilis R&D MOCVD system was used to grow the approximately 1 μm thick epitaxial layer at 880°C with TEGa (triethylgallium) and O_2 precursors. Silane was used as the dopant gas to provide Si for the n-type doping of the sample with a target doping of 1×10^{17} cm^{-3}. The full growth details can be found in prior work by Feng *et al.*[22] The sample went through a "Schottky metal-first" process flow to ensure high quality Schottky contacts for defect spectroscopy techniques. First, the samples were cleaned using acetone, isopropyl alcohol, and de-ionized water before a lift-off process was performed to pattern thin 8 nm Ni Schottky contact that was deposited by electron beam evaporation to a 290 μm $\times$ 290 μm square. The thin metal is required to allow for transmission of light into the epitaxial layer during light-based measurements such as DLOS for trap characterization and internal photoemission for Schottky barrier height measurements. The diodes were then isolated through a mesa etch using BCl_3 and Ar chemistries in an inductively coupled-plasma reactive ion-etcher (ICP-RIE) system down to the substrate. The Ti/Al/Ni/Au Ohmic metal stack was then deposited for top side substrate contacts. The device structure can be seen in the inset of Fig. 1a, and full details of the process flow can be seen in previous reports.[26,27]

III. Results and Discussion

A. Electrical Characteristics

The 1.8 MeV proton radiation was done at Sandia National Laboratories with a beam current of approximately 0.5 μA and a spot size of approximately 3 mm. The expected projected range for the incident protons is approximately 18 μm into the sample based on stopping range of ions in matter (SRIM) simulations.[28] Using transport of ions in matter (TRIM) simulations, a relatively uniform concentration of displacement damage in the form of vacancies and

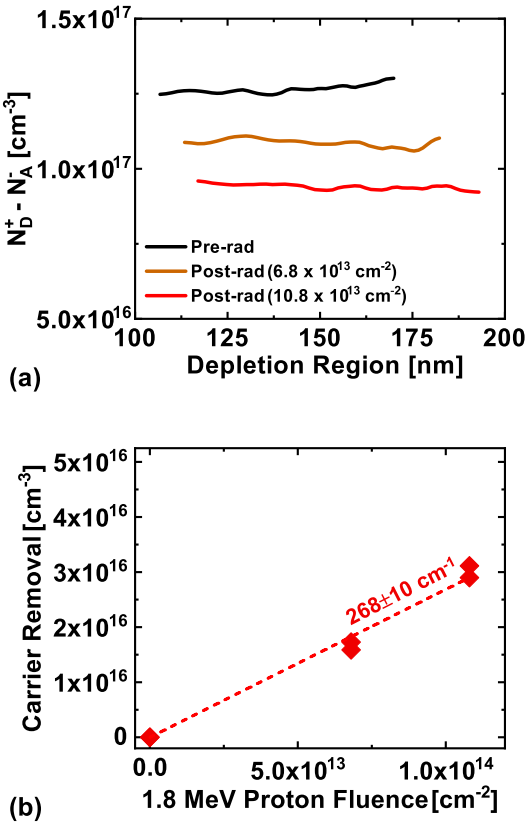

Figure 2. (a) shows the C-V extracted net ionized doping profiles for the same device which indicates there is an increase in carrier compensation due to the radiation damage. The bias range used for each is 0 V to -2 V. (b) characterizes the reduction of carrier concentration as a function of proton fluence with a carrier removal rate of 268$\pm$10 cm^{-1}. This can be used as a metric to understand how hard it is to create damage in the material by radiation where a lower number is more radiation hard.

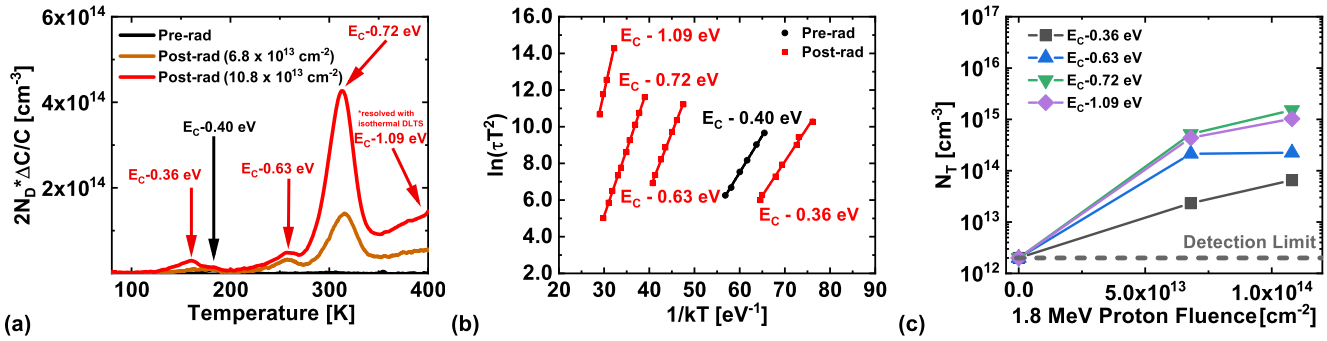

Figure 3. (a) shows the DLTS spectra at each proton fluence point. The pre-radiation scan had only one trap at E_C-0.40 eV indicated by the black arrow while defects introduced by irradiation at E_C-0.36 eV, E_C-0.63 eV, E_C-0.72 eV, and E_C-1.09 eV are indicated by red arrows. The E_C-1.09 eV trap was resolved through the isothermal DLTS technique. (b) shows the Arrhenius data for each defect state using black and red to distinguish as well. (c) shows the trap concentrations as a function of proton fluence which are measured through DLTS.

interstitials in the near-surface active region of the device structure studied here is expected. After each fluence of radiation, the first measurements done were I-V as seen in Fig. 1a. The I-V characteristics show the ideality factor (1.05±0.05) is unaffected, indicating the forward current continues to be dominated by thermionic emission after radiation. The Schottky barrier height (ϕ_B) is extracted from internal photoemission to be 1.40±0.05 eV shown in Fig. 1b, also with no significant change after radiation. With no change in the barrier height or ideality factor, the decrease in the reverse-leakage in Fig. 1a, could be attributed to the lowering of the surface field due to the reduction of $N_D^+ - N_A^-$ (as will be shown) from radiation damage, which could reduce the reverse leakage component from thermionic field emission expected from theoretical models[29], however more work is needed to understand the change in leakage current. The overall reduction in the C-V curve shown in Fig. 1c is a result of a reduction of $N_D^+ - N_A^-$ which can be seen in the C-V extracted doping profiles in Fig. 2a indicating that the net electron concentration is being reduced by increasing proton fluence through the introduction of acceptor-like defect states. Fig. 2b shows the carrier removal, calculated from the reduction in net ionized doping from radiation damage, as a function of proton fluence to extract the carrier removal rate of approximately 268±10 cm^{-1}. This carrier removal rate is about 1.8X lower than the report for GaN[30] under nearly identical radiation conditions and fluences, indicating increased radiation tolerance compared to GaN by this measure and under these conditions. To understand the carrier removal observed from the reduction in the doping profiles, the defects responsible are identified through DLTS and DLOS after each fluence.

B. Impact of Irradiation on DLTS Spectra

The pre-radiation DLTS spectrum for this MOCVD-grown material is shown in Fig. 3a. DLTS data were digitally acquired at high resolution for all transients as a function scan temperature from 77 K to 400 K, and were analyzed using conventional double boxcar methods over a range of rate windows between 4 and 2000 s^{-1} to achieve a high degree of accuracy and confidence in assignment of energy levels. A fill pulse of 0 V and a reverse bias empty pulse of -2 V was used. Compared with prior DLTS studies made on β-Ga_2O_3 grown by other methods, the MOCVD material possesses a very low concentration of traps and here, only a state at E_C-0.40 eV indicated by a black arrow and label, with a capture cross-section of 2×10^{-14} cm^2, is seen above the DLTS detection limit of $\sim2\times10^{12}$ cm^{-3} for this sample. Complete details of the "as-grown" defect spectra can be found in Ghadi *et al.*.[24] Since the pre-radiated trap spectrum is very clean, these devices allow for a precise identification of newly formed defects even at relatively low proton fluences since radiation-induced traps should not be obscured by higher concentrations of pre-existing defects. As seen in Fig. 3a, after the first round of proton irradiation with a fluence of 6.8×10^{13} cm^{-2}, four new trap states detected by DLTS were introduced, as indicated with red arrows. Arrhenius analysis in Fig. 3b shows the radiation induced traps are at energies of E_C-0.36 eV, E_C-0.63 eV, E_C-0.72 eV, and E_C-1.09 eV extracted from the slope with respective apparent capture cross-sections of 7×10^{-15} cm^2, 3×10^{-13} cm^2, 7×10^{-14} cm^2, and 1×10^{-13} cm^2 extracted from the intercept.[31] The isothermal DLTS analysis technique was utilized to resolve the E_C-1.09 eV state since traditional DLTS would have required higher temperatures than possible for our setup during the measurement.[32] Each of these defects has a monotonic increase in concentration suggesting a native point defect related formation is involved. Conversely, the E_C-0.40 eV state does not show an increase for either fluence which indicates that it is likely associated with an extrinsic source; the concentration of extrinsic defects are not expected to increase with radiation because displacement damage cannot introduce additional extrinsic species. No response to radiation could also indicate the defect is an extended defect, however, in the initial study of this material by Ghadi *et al.* the E_C-0.40 eV state DLTS spectrum matched the expected characteristics for a simple point defect.[24] These two pieces of information combined indicate that the source of the E_C-0.40 eV state is likely to be an extrinsic point defect.

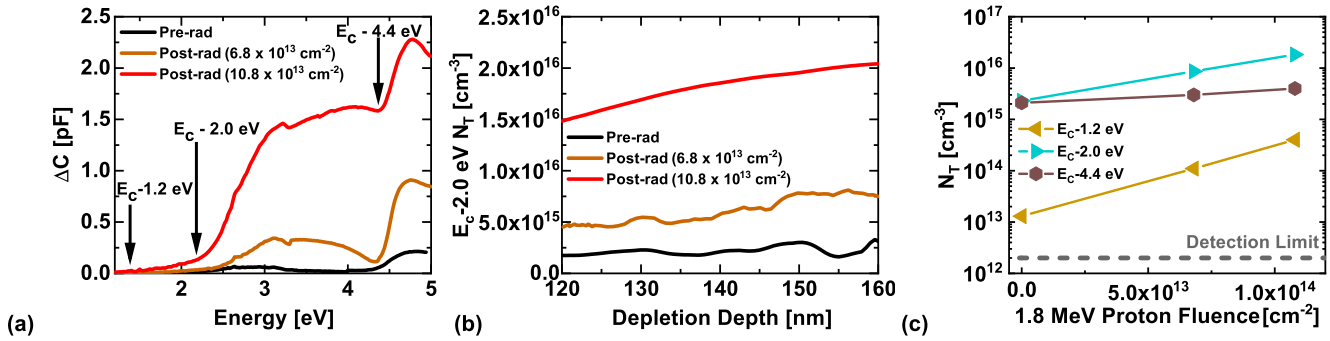

Figure 4. (a) Steady state photocapacitance spectra measured for each proton fluence showing the three traps present before radiation each monotonically increasing. (b) shows the LCV analysis of the E_C-2.0 eV state observed in the SSPC plot to determine the apparent concentrations after each fluence. (c) shows the apparent concentration vs. fluence plot for the trap states which are observed in the DLOS and LCV measurements in the deeper part of the bandgap.

To carefully consider changes in trap concentration, the lambda correction is applied to each DLTS measured trap concentration by accounting for the fraction of the depletion region where the specific deep energy levels are modulated by the DLTS biasing conditions.[33] The lambda-corrected trap concentration is plotted as a function of proton fluence in Fig. 3c. In the upper region of the bandgap that is probed by DLTS, the dominant radiation induced defect is the E_C-0.72 eV state. There have been significant efforts in the community to identify likely sources for the E_C-0.72 eV, also labeled E2*, which has been identified as a source of dispersion in β-Ga_2O_3 transistors.[34,35] Most recently, the defect source is suggested to be related to the acceptor-like $V_{Ga}V_O$ divacancy defect.[36] However, given the complexity of the β-Ga_2O_3 crystal structure, multiple defect configurations result in similarly predicted trap energy levels making correlations between density functional theory (DFT) and experimental results rather difficult.[14,37] Therefore, even though the defect has a clear response to radiation and is likely related to an intrinsic physical source, more work is needed to identify the responsible specific defect configuration.

C. Impact of Irradiation on DLOS Spectra

To fully characterize the defect distribution throughout the β-Ga_2O_3 bandgap, and reveal additional radiation response outside the DLTS measurement range, DLOS and lighted capacitance-voltage (LCV) measurements are done. In DLOS, a Xe-lamp-based monochromatic light source was used to scan incident light from 1.2 eV to 5.0 eV in 0.02 eV steps in order to optically emit electrons that were trapped by deep levels. Prior to optical exposure, traps were filled using a 10 s electrical fill pulse at 0 V. The light exposure was done for 300 s at each energy at a reverse bias of -2 V. Figure 4a shows the steady-state photocapacitance (SSPC) spectra as a function of proton fluence for the same sample used in the DLTS study. The energy levels and Frank-Condon energies (D_{FC}) shown in the figure were extracted from fitting of the optical cross-sections associated with each SSPC step onset energy.[24] Similar to the DLTS results, proton irradiation causes a measurable but non-uniform effect on individual defect states. First, as a baseline, the pre-radiation spectrum (black in the figure) reveals the presence of three deep states, with SSPC onset energies corresponding to the arrows indicated in Fig. 4a. Detailed fitting of the optical cross-sections associated with the SSPC onsets using the Pässler model[38] for the pre-radiated sample was reported previously, which identified the energy levels and their corresponding Frank-Condon energies (D_{FC}) of E_C-1.2 eV (D_{FC}=0.45 eV), E_C-2.0 eV (D_{FC}=0.48 eV), and E_C-4.4 eV (D_{FC}=0.06 eV) as reported in Ghadi *et al.*[24] There is an increase in the E_C-1.2 eV state, however, of the three deep states detected in the DLOS measurement, it has the lowest concentration by approximately two orders of magnitude. Similarly, there is a slight increase observed in the E_C-4.4 eV state that is larger than the shallower states, but it is not the dominant defect present.

The main defect state increasing in concentration is at E_C-2.0 eV, which is apparent from the significant increase in the SSPC plot in Fig. 4a. However, under our SSPC measurement conditions, which uses a light emission measurement time of 300 s at each energy step, it has been previously shown to be insufficient to fully saturate the E_C-2.0 eV trap, leading to an underestimation of trap concentration determined only from our standard SSPC measurements.[12,39] This was attributed to a small optical cross-section for this state such that the product of the photon flux and optical cross-section (which equals the electron optical emission rate) leads to incomplete saturation of this state. In fact, this also causes the downward trend in the SSPC for this state at higher photon energies (as seen in Fig. 4a) due to the Xe arc lamp's photon flux reducing in this energy range. To mitigate this effect, we applied the LCV method[40], with which the light exposure duration can be significantly increased to saturate the capacitance signal associated with trap emission. LCV measurements are done by performing CV measurements before (dark; before trap emission) and after (after trap emission) light exposure at specific photon energies that are informed by the SSPC onset energies. The time of light exposure required depends on the specific trap characteristics until a stable saturation of ΔC

is achieved, which for the E_C-2.0 eV state required a three hour exposure, well beyond the 300 s exposure used in the DLOS and SSPC measurements. The LCV results after each fluence for the E_C-2.0 eV state using the difference between the C-V net ionized doping ($N_D^+ - N_A^-$) measured in the dark and after a three hour light exposure to saturate ΔC are shown in Fig. 4b. The change in the concentration is plotted over the same depletion region so that the same traps are modulated in each LCV scan.

The defects in the lower part of the bandgap measured through DLOS and LCV have higher concentrations over those measured using DLTS by two orders of magnitude in the pre-radiation spectrum and continue to dominate after radiation. The concentrations of the states detected through DLOS are plotted as a function of proton fluence in Fig. 4c with the SSPC extracted concentration for the E_C-1.2 eV and E_C-4.4 eV states and LCV extracted concentration for the E_C-2.0 eV state. The E_C-4.4 eV state shows an increase in concentration, but the E_C-2.0 eV dominates the introduction rate accounting for ~75% of all increased defect concentrations. The dominating response to radiation observed in the E_C-2.0 eV state has also been observed in neutron radiated β-Ga_2O_3 in previous work indicating the source is likely due to an intrinsic defect formation.[12,39] As stated above, the precise defect configurations for a crystal structure as complex as β-Ga_2O_3 is a non-trivial undertaking. The E_C-2.0 eV state has been linked to an acceptor-like gallium divacancy-interstitial complexes ($2V_{Ga}$-Ga_i) through high resolution transmission electron microscopy and the relevant DFT calculations for both the i_b and i_c sites.[12,39,41] Although this connection does not directly identify the source of the E_C-2.0 eV state, it does provide a likely candidate.[41] As summarized by Farzana *et al.*, other candidates could be the predicted acceptor-like isolated Ga vacancies (V_{Ga}^{I} and V_{Ga}^{II}) and hydrogenated Ga vacancy complexes (V_{Ga}-H_I, V_{Ga}-H_{II}, V_{Ga}^{ic}-H, V_{Ga}^{ib}-2H, and V_{Ga}^{ic}-2H).[12,14,42,43]

In previous studies based on other growth methods[12,39], the E_C-4.4 eV state did not show a measurable increase in concentration after radiation; the results here indicate a measurable increase in concentration which may have been overshadowed in previous work where the initial concentration was nearly an order of magnitude higher. Therefore, the E_C-4.4 eV state might involve an intrinsic defect source. More work needs to be done to understand the defect responsible for this state; the MOCVD material with a low concentrations of defects may be useful to increase the sensitivity of changes in this state.

D. Understanding Defects Responsible for Irradiation-induced Compensation

A diagrammatic representation of the distribution of bandgap states is given in Fig. 5. In an attempt to understand which of the traps measured are responsible for the observed carrier reduction in Fig. 2b, the individual trap introductions are calculated for each fluence, where the trap introduction rate shown in Fig. 6a is calculated similarly to the carrier removal rate. Of the defects created or increasing in concentration from radiation the E_C-2.0 eV state is dominating with an introduction rate accounting for ~75% of the total introduction rate as seen in Fig. 6a, with the other six traps

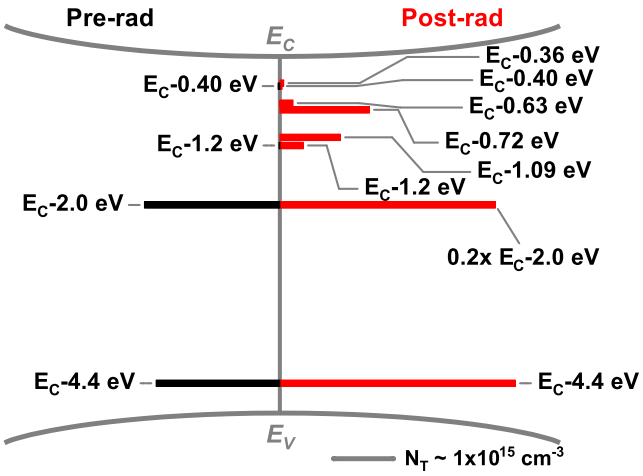

Figure 5. Summary of the distribution of deep level defect states detected by DLTS, DLOS, and LCV before irradiation and after irradiation at a proton fluence of 10.8×10^{13} cm^{-2}. Note that the E_C-2.0 eV state is shown at 0.2X the actual concentration and the scale bar applies to both conditions.

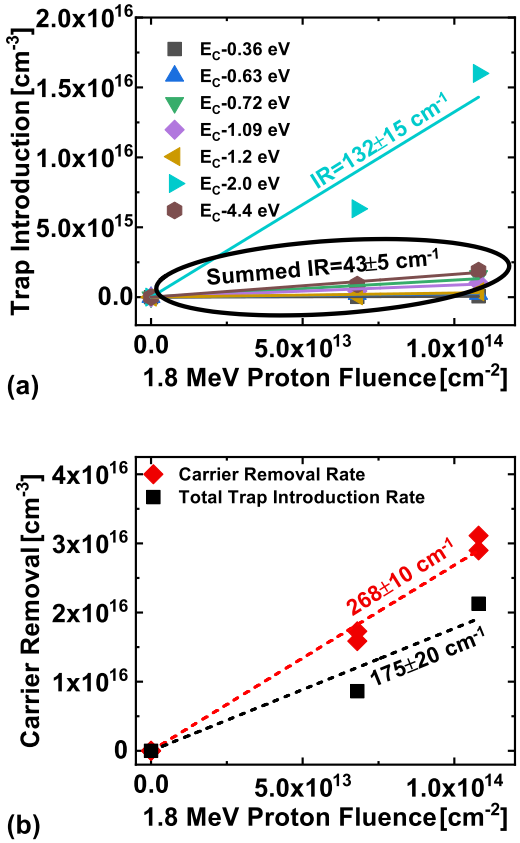

Figure 6. (a) shows the individual trap introduction concentrations as a function of proton fluence to determine the individual trap introduction rates (IR). (b) shows the carrier removal and total trap concentrations as a function of fluence to directly compare both the carrier removal and total trap introduction rates.

accounting for the remainder as shown. This, coupled with the expected acceptor-like nature of its potential sources observed in positron annihilation studies[44,45] and calculated from DFT[12,39,41] described above strongly suggests it is the main compensating defect. The E_C-0.72 eV state comprises ∼7% of the total trap introduction rate and also contributes to compensation due its expected acceptor-like nature.[36] The five other deep levels account for the remaining ∼18% of the introduced defects. It is not clear if these levels contribute to the compensation, as their physical configurations are not confidently identified and could be donor-like in nature.

The carrier removal and total trap introduction rate comparison for the MOCVD sample extracted from the C-V, and the DLTS/DLOS/LCV results is shown in Fig. 6b. There is reasonable agreement between the removal rate and the total introduction rate, indicating the dominance of radiation-induced acceptor-like deep levels acting to strongly compensate the net electron concentration. However, we emphasize that the trap introduction rate for the dominant E_C-2.0 eV state is likely to be underestimated since the 4 eV photons used by LCV to stimulate electron emission from the E_C-2.0 eV state to the conduction band, can also optically emit holes to the valence band. This results in a steady state condition (based on a balance between electron and hole emission rates) where only a fraction of the total trap concentration is ionized[33], therefore leading to an underestimation of the total trap concentration in this particular condition. Future work to remove the underestimation is underway, but this does not change the fact that this trap is the dominant source of carrier removal.

IV. Conclusions

In conclusion, the impact of 1.8 MeV proton radiation on MOCVD-grown β-Ga_2O_3 Schottky diodes and the defect spectrum throughout the bandgap is characterized. The I-V characteristics show a reduction in leakage current with an unchanged ideality factor of 1.05±0.05. IPE indicates the Schottky barrier height remains unchanged at 1.40±0.05 eV. The C-V extracted net ionized doping is reduced as a function of proton fluence with a carrier removal rate of 268±10 cm^{-1}. Of the defects created by proton irradiation, both of the dominating states match previous theoretical predictions[12,36,39,41] attributing their sources to acceptor-like gallium vacancies. The E_C-0.72 eV trap had the largest impact on the DLTS spectrum, however, the deeper V_{Ga} related state at E_C-2.0 eV is determined to be the most significant contribution accounting for ∼75% of the total introduction rate. The complete bandgap defect characterization of radiation damage done here can be used to understand and model the impact of radiation on a range of devices for radiation tolerant device designs.

Acknowledgements

The authors acknowledge the funding support from Air Force Office of Scientific Research No. FA9550-18-1-0479 (Ali Sayir, Program Manager). The authors also acknowledge the funding support from the Department of the Defense, Defense Threat Reduction Agency, Grant No. HDTRA11710034 (Jacob Calkins, Program Manager). This work was also sponsored by the NSF Graduate Research Fellowship Program under Grant No. DGE-1343012. This work was supported in part by the US Air Force Radiation Effects Center of Excellence, Grant No. FA9550-22-1-0012. Any opinions, findings, and conclusions or recommendations expressed in this material are those of the authors and do not necessarily reflect the views of the funding provider. Sandia National Laboratories is a multi-mission laboratory managed and operated by National Technology & Engineering Solutions of Sandia, LLC, a wholly owned subsidiary of Honeywell International Inc., for the U.S. Department of Energy's National Nuclear Security Administration under contract DE-NA0003525. The views expressed in the article do not necessarily represent the views of the U.S. Department of Energy or the U.S. Government.

References

[1] Z. Galazka, K. Irmscher, R. Uecker, R. Bertram, M. Pietsch, A. Kwasniewski, M. Naumann, T. Schulz, R. Schewski, D. Klimm, and M. Bickermann, Journal of Crystal Growth **404**, 184 (2014).
[2] E. G. Villora, K. Shimamura, Y. Yoshikawa, T. Ujiie, and K. Aoki, Applied Physics Letters **92**, 202120 (2008).
[3] H. Aida, K. Nishiguchi, H. Takeda, N. Aota, K. Sunakawa, and Y. Yaguchi, Japanese Journal of Applied Physics **47**, 8506 (2008).
[4] N. Ueda, H. Hosono, R. Waseda, and H. Kawazoe, Applied Physics Letters **70**, 3561 (1997).
[5] H. H. Tippins, Physical Review **140**, A316 (1965).
[6] M. R. Lorenz, J. F. Woods, and R. J. Gambino, Journal of Physics and Chemistry of Solids **28**, 403 (1967).
[7] M. Higashiwaki, K. Sasaki, A. Kuramata, T. Masui, and S. Yamakoshi, Applied Physics Letters **100**, 013504 (2012).
[8] Z. Hu, K. Nomoto, W. Li, N. Tanen, K. Sasaki, A. Kuramata, T. Nakamura, D. Jena, and H. G. Xing, IEEE Electron Device Letters **39**, 869 (2018).
[9] A. J. Green, K. D. Chabak, E. R. Heller, R. C. Fitch, M. Baldini, A. Fiedler, K. Irmscher, G. Wagner, Z. Galazka, S. E. Tetlak, A. Crespo, K. Leedy, and G. H. Jessen, IEEE Electron Device Letters **37**, 902 (2016).
[10] C. Joishi, S. Rafique, Z. Xia, L. Han, S. Krishnamoorthy, Y. Zhang, S. Lodha, H. Zhao, and S. Rajan, Applied Physics Express **11**, 031101 (2018).
[11] A. Ionascut-Nedelcescu, C. Carlone, A. Houdayer, H. J. von Bardeleben, J. Cantin, and S. Raymond, IEEE Transactions on Nuclear Science **49**, 2733 (2002).
[12] E. Farzana, A. Mauze, J. B. Varley, T. E. Blue, J. S. Speck, A. R. Arehart, and S. A. Ringel, APL Materials **7**, 121102 (2019).
[13] M. E. Ingebrigtsen, J. B. Varley, A. Y. Kuznetsov, B. G. Svensson, G. Alfieri, A. Mihaila, U. Badstübner, and L. Vines, Applied Physics Letters **112**, 042104 (2018).
[14] M. E. Ingebrigtsen, A. Y. Kuznetsov, B. G. Svensson, G. Alfieri, A. Mihaila, U. Badstübner, A. Perron, L. Vines, and J. B. Varley, APL Materials **7**, 022510 (2018).
[15] J. Yang, Z. Chen, F. Ren, S. J. Pearton, G. Yang, J. Kim, J. Lee, E. Flitsiyan, L. Chernyak, and A. Kuramata, Journal of Vacuum Science & Technology B **36**, 011206 (2018).
[16] A. Y. Polyakov, N. B. Smirnov, I. V. Shchemerov, E. B. Yakimov, S. J. Pearton, C. Fares, J. Yang, F. Ren, J. Kim, P. B. Lagov, V. S. Stolbunov, and A. Kochkova, Applied Physics Letters **113**, 092102 (2018).
[17] A. Y. Polyakov, N. B. Smirnov, I. V. Shchemerov, E. B. Yakimov, J. Yang, F. Ren, G. Yang, J. Kim, A. Kuramata, and S. J. Pearton, Applied Physics Letters **112**, 032107 (2018).
[18] A. Y. Polyakov, N. B. Smirnov, I. V. Shchemerov, A. A. Vasilev, E. B. Yakimov, A. V. Chernykh, A. I. Kochkova, P. B. Lagov, Y. S. Pavlov, O. F. Kukharchuk, A. A. Suvorov, N. S. Garanin, I.-H. Lee, M. Xian, F. Ren, and S. J. Pearton, Journal of Physics D: Applied Physics **53**, 274001 (2020).
[19] J. Yang, F. Ren, S. J. Pearton, G. Yang, J. Kim, and A. Kuramata, Journal of Vacuum Science & Technology B **35**, 031208 (2017).
[20] S. Ahn, Y.-H. Lin, F. Ren, S. Oh, Y. Jung, G. Yang, J. Kim, M. A. Mastro, J. K. Hite, C. R. Eddy, and S. J. Pearton, Journal of Vacuum Science &

Technology B **34**, 041213 (2016).
[21] J. Lee, E. Flitsiyan, L. Chernyak, J. Yang, F. Ren, S. J. Pearton, B. Meyler, and Y. J. Salzman, Applied Physics Letters **112**, 082104 (2018).
[22] Z. Feng, A. F. M. Anhar Uddin Bhuiyan, M. R. Karim, and H. Zhao, Applied Physics Letters **114**, 250601 (2019).
[23] Z. Feng, A. F. M. A. U. Bhuiyan, Z. Xia, W. Moore, Z. Chen, J. F. McGlone, D. R. Daughton, A. R. Arehart, S. A. Ringel, S. Rajan, and H. Zhao, physica status solidi (RRL) – Rapid Research Letters **14**, 2000145 (2020).
[24] H. Ghadi, J. F. McGlone, C. M. Jackson, E. Farzana, Z. Feng, A. F. M. A. U. Bhuiyan, H. Zhao, A. R. Arehart, and S. A. Ringel, APL Materials **8**, 021111 (2020).
[25] H. Ghadi, J. F. McGlone, Z. Feng, A. F. M. A. U. Bhuiyan, H. Zhao, A. R. Arehart, and S. A. Ringel, Applied Physics Letters **117**, 172106 (2020).
[26] Z. Zhang, E. Farzana, A. R. Arehart, and S. A. Ringel, Applied Physics Letters **108**, 052105 (2016).
[27] E. Farzana, E. Ahmadi, J. S. Speck, A. R. Arehart, and S. A. Ringel, Journal of Applied Physics **123**, 161410 (2018).
[28] J. F. Ziegler, M. D. Ziegler, and J. P. Biersack, Nuclear Instruments and Methods in Physics Research Section B **268**, 1818 (2010).
[29] W. Li, D. Jena, and H. G. Xing, Journal of Applied Physics **131**, 015702 (2022).
[30] Z. Zhang, D. Cardwell, A. Sasikumar, E. C. H. Kyle, J. Chen, E. X. Zhang, D. M. Fleetwood, R. D. Schrimpf, J. S. Speck, A. R. Arehart, and S. A. Ringel, Journal of Applied Physics **119**, 165704 (2016).
[31] D. V. Lang, Journal of Applied Physics **45**, 3023 (1974).
[32] V. I. Turchanikov, V. S. Lysenko, and V. A. Gusev, physica status solidi (a) **95**, 283 (1986).
[33] P. Blood and J. W. Orton, *The Electrical Characterization of Semiconductors: Majority Carriers and Electron States* (Academic Press Limited, San Diego, CA, 1992).
[34] J. F. McGlone, Z. Xia, Y. Zhang, C. Joishi, S. Lodha, S. Rajan, S. A. Ringel, and A. R. Arehart, IEEE Electron Device Letters **39**, 1042 (2018).
[35] J. F. McGlone, Z. Xia, C. Joishi, S. Lodha, S. Rajan, S. Ringel, and A. R. Arehart, Applied Physics Letters **115**, 153501 (2019).
[36] Y. K. Frodason, C. Zimmermann, E. F. Verhoeven, P. M. Weiser, L. Vines, and J. B. Varley, Physical Review Materials **5**, 025402 (2021).
[37] P. Deák, Q. Duy Ho, F. Seemann, B. Aradi, M. Lorke, and T. Frauenheim, Physical Review B **95**, 075208 (2017).
[38] R. Pässler, Journal of Applied Physics **96**, 715 (2004).
[39] E. Farzana, M. F. Chaiken, T. E. Blue, A. R. Arehart, and S. A. Ringel, APL Materials **7**, 022502 (2018).
[40] A. Armstrong, A. R. Arehart, and S. A. Ringel, Journal of Applied Physics **97**, 083529 (2005).
[41] J. M. Johnson, Z. Chen, J. B. Varley, C. M. Jackson, E. Farzana, Z. Zhang, A. R. Arehart, H.-L. Huang, A. Genc, S. A. Ringel, C. G. Van de Walle, D. A. Muller, and J. Hwang, Physical Review X **9**, 041027 (2019).
[42] J. B. Varley, H. Peelaers, A. Janotti, and C. G. Van de Walle, Journal of Physics: Condensed Matter **23**, 334212 (2011).
[43] P. Weiser, M. Stavola, W. B. Fowler, Y. Qin, and S. Pearton, Applied Physics Letters **112**, 232104 (2018).
[44] A. Karjalainen, I. Makkonen, J. Etula, K. Goto, H. Murakami, Y. Kumagai, and F. Tuomisto, Applied Physics Letters **118**, 072104 (2021).
[45] A. Karjalainen, P. M. Weiser, I. Makkonen, V. M. Reinertsen, L. Vines, and F. Tuomisto, Journal of Applied Physics **129**, 165702 (2021).